https://doi.org/10.5194/gmd-2021-436
Preprint. Discussion started: 10 January 2022
© Author(s) 2022. CC BY 4.0 License.

Geoscientific Model Development Discussions

The bulk parameterizations of turbulent air-sea fluxes in NEMO4: the origin of Sea Surface Temperature differences in a global model study

Giulia Bonino[1*], Doroteaciro Iovino[1], Laurent Brodeau[2], and Simona Masina[1]

[1]Ocean Modeling and Data Assimilation Division, Centro Euro-Mediterraneo sui Cambiamenti Climatici, Bologna, Italy.
[2]Centre National de la Recherche Scientifique, IGE/MEOM, Grenoble, France

Correspondence: Giulia Bonino (giulia.bonino@cmcc.it)

Abstract.
Wind stress and turbulent heat fluxes are the major driving forces which modify the ocean dynamics and thermodynamics. In the NEMO ocean general circulation model, these turbulent air-sea fluxes (TASFs), which are components of the ocean model boundary conditions, can critically impact the simulated ocean characteristics. This paper investigates how the different bulk parametrizations to calculated turbulent air-sea fluxes in the NEMO4 (revision 12957) drives substantial differences in sea surface temperature (SST). Specifically, we study the contribution of different aspects and assumptions of the bulk parametrizations in driving the SST differences in NEMO global model configuration at ¼ degree of horizontal resolution. These include the use of the skin temperature instead of the bulk SST in the computation of turbulent heat flux components, the estimation of wind stress and the estimation of turbulent heat flux components which vary in each parametrization due to the different computation of the bulk transfer coefficients. The analysis of a set of short-term sensitivity experiments, where the only experimental change is related to one of the aspects of the bulk parametrizations, shows that parametrization-related SST differences are primarily sensitive to the wind stress differences across parametrizations and to the implementation of skin temperature in the computation of turbulent heat flux components. Moreover, in order to highlight the role of SST-turbulent heat flux negative feedback at play in ocean simulations, we compare the TASFs differences obtained using NEMO ocean model with the estimations from Brodeau et al. (2017), who compared the different bulk parametrizations using prescribed SST. Our estimations of turbulent heat flux differences between bulk parametrizations is weaker with respect to Brodeau et al. (2017) differences estimations.

1 Introduction

Ocean and atmosphere circulations are highly influenced by the transfer of momentum and heat at the air-sea interface (e.g., Gill, 1982; Siedler et al., 2013). These transfers of energy are primarily driven by turbulent air–sea fluxes (TASFs), which include wind stress and the turbulent heat flux components (THFs, latent and sensible heat fluxes). In the upper ocean, the wind stress is a major driving force for basin-scale circulation (e.g., Chen et al., 1994; Shriver and Hurlburt, 1997), and the THFs are important for determining its thermal properties (e.g., Yuen et al., 1992; Swenson and Hansen, 1999). Therefore,

https://doi.org/10.5194/gmd-2021-436
Preprint. Discussion started: 10 January 2022
© Author(s) 2022. CC BY 4.0 License.

both wind stress and THFs are important for the evolution of sea surface temperature (SST), because of their contribution to turbulent mixing within the ocean surface mixed layer (e.g., Barnier, 1998).

Since direct observations of TASFs are sparse in space and time, the estimates of TASFs are derived using bulk formulas, which relate each component of turbulent air-sea flux to more easily measurable and widely available meteorological surface state variables (e.g. wind speed, air temperature, air specific humidity) through bulk transfer coefficient. These bulk transfer coefficients are estimated using bulk parametrizations. Different bulk parametrizations are currently used and they are traditionally developed statistically, comparing in situ meteorological observations of surface state variables with TASFs derived from ship and buoy measurements (Large and Pond, 1981, 1982; Smith, 1988; Fairall et al., 1996, 2003; Bradley and Fairall, 2007).

In NEMO ocean general circulation model, TASFs, which are components of the ocean boundary conditions, are computed by means of bulk formulas using prescribed surface atmospheric state variables (air temperature, air humidity, wind) and the prognostic SST of the model (hereinafter online prognostic SST approach). The online prognostic SST approach allows that the response of the ocean (i.e. SST) to atmospheric events is incorporated into the estimation of the THFs and of longwave radiation (i.e. non solar heat flux components, NSHFs) at every time step of the numerical experiment. The possibility of feedback mechanisms between the ocean and the atmosphere partially simulate the energy exchange between the atmosphere and ocean (Kara et al., 2000). The approach requires the choice of a given bulk parameterization, which influences the magnitude of the wind stress and of the THFs (Kara et al., 2000). These TASFs affect the simulated ocean characteristics and in particular the evolution of the SST (Torres et al., 2019).

Brodeau et al. (2017) compared a set of bulk parametrizations computing TASFs using prescribed SST (hereinafter offline prescribed SST approach) rather than prognostic SST of the model. Based on their approach Brodeau et al. (2017) report that the use of different bulk parametrizations to estimate TASFs can typically produce differences in total turbulent heat flux (Q_T, i.e. the sum of the THFs, latent and sensible heat fluxes) of about $10W/m^2$ and in wind stress of about $20mN/m^2$. The online prognostic SST approach, used by the NEMO experiments performed for this study, can substantially modify these estimations. The SST feeds back negatively on the Q_T likely damping the Q_T discrepancies across the different bulk parametrizations (Seager et al., 1995).

The purpose of this work is to better understand the response of the prognostic SST to the TASFs and to their parametrization in NEMO version 4.0 at 1/4° of horizontal resolution, and to discuss the role of the SST-Q_T negative feedback at play in the online prognostic SST approach. We address the sensitivity of the SST to various aspects of the different bulk parametrizations such as the inclusion of the skin temperature in the computation of the THFs and the role of the bulk transfer coefficients in the estimation of the wind stress and the THFs. In order to do that, we analysed differences between short-term sensitivity experiments where bulk assumptions are excluded (e.g skin temperature) or bulk transfer coefficients are computed mixing the different bulk parametrizations. Lastly, in order to highlight the role of the SST-Q_T negative feedback at play in our online prognostic SST approach, we compare the TASFs with the estimations from Brodeau et al. (2017). The validation of modeled SST against observed datasets is beyond the scope of this study. Here, the main objective is to investigate the impact of a set of bulk parametrizations on the SST generated by NEMO rather than evaluate their accuracy in reproducing it.

This paper is organized as follows: in section 2, we present the model used for this study, a short overview of the bulk formulas implemented in NEMO4, the experimental set-up and the modifications introduced in the bulk parametrizations to performed sensitivity experiments. In section 3 we present the parametrization-related SST discrepancies, we quantify SST discrepancies related to various aspects of the different bulk parametrizations and we compare and discuss our finding in relation to existing works. Our conclusions are summarized in section 5.

2 Model configuration, bulk forcing and experimental set-up

2.1 NEMO4 model configuration

The sensitivity of prognostic SST to bulk parametrizations is investigated in a numerical study using the Nucleus for European Modelling of the Ocean[1] (NEMO, version 4.0, revision 12957). NEMO is a three-dimensional, free-surface, hydrostatic, primitive-equation global ocean general circulation model (Madec G. and NEMO System Team, 2019) coupled to the Sea Ice modelling Integrated Initiative (SI^3, NEMO Sea Ice Working Group, 2020). Our configuration uses the global ORCA025 tripolar grid (Madec and Imbard, 1996) with 1/4° horizontal resolution (27.75km) at the Equator, which increases with latitudes, e.g. 14km at 60 °. The vertical grid has 75 levels, whose spacing increases with a double hyperbolic tangent function of depth from 1 m near the surface to 200 m at the bottom, with partial steps representing the bottom topography (Bernard et al., 2006). The model bathymetry is based on the combination of ETOPO1 data set (Amante and Eakins, 2009) in the open ocean and GEBCO (IOC, 2003) in coastal regions. The horizontal turbulent viscosity is parameterized by means of a biharmonic function with a value of $1.8 \times 10^{11} m^4 s^{-1}$ at the Equator, reducing poleward as the cube of the maximum grid cell size. The advection of the tracers uses a total variance dissipation (TVD) scheme (Zalesak, 1979). The laplacian lateral tracer mixing is along isoneutral surfaces with a coefficient of 300 $m^2 s - 1$. The vertical mixing of tracers and momentum is parameterised using the turbulent kinetic energy (TKE) scheme (Marsaleix et al., 2008). Subgrid-scale vertical mixing processes are represented by a background vertical eddy diffusivity of $1.2 \times 10^{-5} m^2 s^{-1}$ and a globally constant background viscosity of $1.2 \times 10^{-4} m^2 s^{-1}$. The bottom friction is quadratic and a diffusive bottom boundary layer scheme is included. The continental runoff data are a monthly climatology derived from the global river flow and continental discharge data set for the major rivers (Dai and Trenberth, 2002; Dai et al., 2009), and estimates by Jacobs et al. (1996) for the Antarctic coastal freshwater discharge. The initial conditions for temperature and salinity are provided by World Ocean Atlas 2013 (Levitus et al., 2013). All the experiments are forced with the hourly ERA5 Reanalysis of the ECMWF (Hersbach, 2016).

[1] https://www.nemo-ocean.eu/

https://doi.org/10.5194/gmd-2021-436
Preprint. Discussion started: 10 January 2022
© Author(s) 2022. CC BY 4.0 License.

2.2 The bulk formulas and their parametrization in NEMO4.0

As stated in the introduction, NEMO uses the online prognostic SST approach to compute TASFs, which are calculated using the prognostic SST and prescribed atmospheric surface state variables by means of aerodynamic bulk formulas:

$$\tau = \rho C_D u \mathbf{u_z} \tag{1a}$$

$$Q_H = \rho C_p C_H (\theta_z - T_s) U \tag{1b}$$

$$E = \rho C_E (q_0 - q_z) U \tag{1c}$$

$$Q_L = -L_v E \tag{1d}$$

where τ is the wind stress, Q_H is the turbulent flux of sensible heat , E is the evaporation, and Q_L is the turbulent flux of latent heat. Throughout this paper, we use the convention that a positive sign of τ, of THFs Q_H and Q_L, and of the total turbulent heat flux Q_T ($Q_T = Q_H + Q_L$) means a gain of the relevant quantity for the ocean. The term ρ is the density of air; C_p is the heat capacity of moist air, and L_v is the latent heat of vaporization. $\mathbf{u_z}$ is the wind speed vector at height z, possibly referred to the ocean currents. The bulk scalar wind speed U is the scalar wind speed $|\mathbf{u_z}|$ with the potential inclusion of a gustiness contribution. The convective gustiness is a temporary increased of the wind speed due to the friction and the free convection and it is active and significant in very calm wind conditions with unstable near-surface atmosphere. It is added to the wind speed and it avoids the zero wind singularity. θ_z and q_z are the potential temperature and the specific humidity of air at height z, while T_s, q_0 are he potential temperature and specific humidity at surface. Depending on the bulk parametrization used, T_s can be the temperature at the air-sea interface (sea surface skin temperature, SSTskin) or at typically 1 meter deep (bulk sea surface temperature, SST). The SSTskin differs from the SST due to the contributions of two effects of opposite sign: the cool skin and warm layer (CSWL). The cool skin is millimeter-scale uppermost layer of the ocean where a vertical gradient of temperature exists to sustain the heat flux continuity between ocean and atmosphere. The warm layer is the warming of the upper few meters of the ocean under day and sunny conditions. C_D, C_H, and C_E are the Bulk Transfer Coefficients (BTCs) for wind stress, sensible heat, and moisture, respectively.

Therefore, the main differences among bulk parametrizations are usually related to:

1. The use of the skin temperature (hereinafter SSTskin) rather than the bulk SST in the estimation of near surface atmospheric stability and bulk formulas.
2. Inclusion of convective gustiness in wind calculation

https://doi.org/10.5194/gmd-2021-436
Preprint. Discussion started: 10 January 2022
© Author(s) 2022. CC BY 4.0 License.

3. The bulk transfer coefficients

The online prognostic SST approach of NEMO allows the air-sea feedback mechanism. The estimation of the NSHFs is indeed influenced by the prognostic SST at each time step. In our experiments, we only focus on the NSHFs computed by bulk formulas, namely the THFs. The SST is responding to the total turbulent heat flux Q_T at each time step: the Q_T generate SST anomalies, and SST anomalies, in turn, can modulate Q_T. Specifically, SST and Q_T feedback negatively: when the SST gets anomalously cold, then Q_T increases, and that means that as a response to increased Q_T, the SST will tend to increase and the Q_T to decrease and so on. This negative feedback of the online prognostic SST works to reduce the heat fluxes divergence across the different bulk parametrizations. On the other hand, the wind stress is not affected by the this type of first-order feedback at play for the Q_T.

In this study we focus on three of bulk parametrizations implemented in NEMO4: NCAR (Large and Yeager, 2009), COARE 3.6 (Edson et al., 2013) (hereinafter referred to as "COARE"), and ECMWF as the version of the bulk parametrization used in the recent cycles of the Integrated Forecast System (IFS) developed at ECMWF, such as cycle 41 (ECMWF, 2015).
COARE and ECMWF parametrizations are meant to be used with the SSTskin, so that the two algorithms include a CSWL parameterization to estimate SSTskin. NCAR uses the bulk SST in heat fluxes calculation and the zero wind singularity is avoided by simply setting a minimum value for the scalar wind speed to $0.5 m/s$. To calculate the BTCs, the bulk parametrizations rely on an empirical closure. More specifically, in COARE and ECMWF parametrizations, the computation of BTCs relies on the Monin-Obukhov similarity theory (MOST, Monin and Obukhov, 1954). As such, BTCs are function of the roughness lengths and of the stability of the atmospheric surface layer. The NCAR parametrization, instead of parametrizing the roughness lengths, parametrizes the BTCs directly as functions of neutral wind speed (e.g. the wind speed at neutral stability condition and at 10m reference level, U_{N10}) before shifting them to the current atmospheric stability. Figure 1 shows the

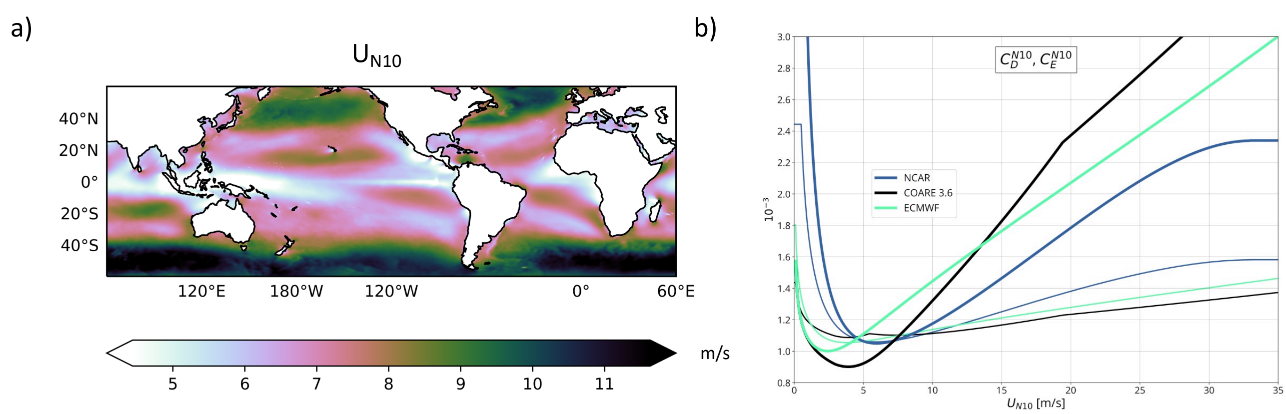

Figure 1. a) Annual mean of U_{N10} from NCAR parametrization b) Neutral drag and moisture transfer coefficients for COARE (black), NCAR (blue), and ECMWF (green) bulk parametrizations (thick and thin lines, respectively), as functions of the neutral wind speed at 10 m.

https://doi.org/10.5194/gmd-2021-436
Preprint. Discussion started: 10 January 2022
© Author(s) 2022. CC BY 4.0 License.

U_{N10} annual mean and the neutral BTCs as a function of of U_{N10} for the selected bulk formula parametrizations. Due to the stronger neutral drag coefficient C_D^{N10}, NCAR parametrization tends to promote wind stress with respect to COARE and to lower extend to ECMWF under light wind condition ($u < 5m/s$). On the other hand, ECMWF parametrization promotes wind stress with respect to NCAR and COARE for wind speed above $5m/s$, while COARE enhances it for wind speed above $13m/s$. For the discussion of the following results, it is important to highlight the wind speed range where the NCAR C_D^{N10} function intersect with ECMWF and COARE C_D^{N10} functions. In the range of 7-9 m/s the C_D^{N10} of COARE is smaller than ECMWF, but slightly higher or approximately equal (around 7 m/s) than NCAR C_D^{N10}. In the range of 4-5 m/s the C_D^{N10} of ECMWF is slightly smaller or approximately equal than NCAR, but higher than COARE C_D^{N10}. Under all conditions NCAR parametrization tends to enhance evaporation with respect to COARE and ECMWF, due to the stronger C_E^{N10} (see Figure 1). For detailed explanation of BTCs derivation for each bulk parametrizations please refer to the technical report by Bonino et al. (2020).

2.3 Experimental set-up

In order to investigate the role of different aspects of bulk parametrizations in driving prognostic SST, we performed five numerical experiments (Table 1). All the experiments are 1 year long experiments, forced by the hourly surface atmospheric state of the ERA5 Weather Reanalysis (Hersbach, 2016). We first performed three experiments (hereinafter 'control experiments') in order to quantify the bulk parametrization-related SST discrepancies:

1. Experiment **ECMWF_S**:uses the ECMWF parametrization. THFs are computed with the SSTskin estimated from CSWL scheme. The parametrization es the absolute wind speed.

2. Experiment **COARE_S**: uses the COARE parametrization. THFs are computed with the SSTskin estimated from CSWL scheme. The parametrization uses the absolute wind speed.

3. Experiment **NCAR**: uses the NCAR parametrization. The parametrization does not include the currents correction in the wind calculation. THFs are computed with the bulk SST, as opposed to `ECMWF_S` and `COARE_S` that use the SSTskin (through their respective CSWL scheme).

In order to disentangle the contribution of the skin temperature and the contribution of the different wind stress and THFs in driving sea surface temperature differences, we performed two sensitivity experiments (hereinafter 'mixed experiments'):

1. Experiment **ECMWF_NS**:uses the ECMWF parametrization. THFs are computed with the bulk SST rather than SSTskin. The parametrization uses the absolute wind speed.

2. Experiment **CdNCAR_CeEC**: uses the ECMWF parametrization to calculate C_H and C_E BTCs and the NCAR bulk formula to calculate C_D BTC. The parametrization do not include the Cool Skin Warm Temperature scheme. The parametrization uses the absolute wind speed.

https://doi.org/10.5194/gmd-2021-436
Preprint. Discussion started: 10 January 2022
© Author(s) 2022. CC BY 4.0 License.

First, the comparison between ECMWF_S and ECMWF_NS is used to determine the Skin Temperature contribution in driving THFs differences and in turn SST differences. Second, the comparison between CdNCAR_CeEC and ECMWF_NS, which differ only for the C_D BTC computation, and between CdNCAR_CeEC and NCAR, which differ only for the C_H and C_E BTCs computation, teach us about the wind stress and the THFs differences contribution in driving SST differences, respectively. We analyze annual mean differences between experiments. We use the absolute wind (e.g. the parametrizations do not include the currents feedback to calculate wind in equation 1a) for the sake of simplicity.

	sea surface temperature used (T_s)	computation of C_D	computation of C_E and C_H
COARE_S	SSTskin	COARE3.6	COARE3.6
ECMWF_S	SSTskin	ECMWF	ECMWF
NCAR	SST	NCAR	NCAR
ECMWF_NS	SST	ECMWF	ECMWF
CdNCAR_CeEC	SST	NCAR	ECMWF

Table 1. Summary of the numerical experiments.

3 Results

In the following sections we discuss the parametrization-related SST discrepancies in the "control experiments" (section 3.1) and we describe the sensitivity of the prognostic SST of the model to various aspects of the bulk parameterizations. These include the use of the skin temperature instead of the bulk SST in the computation of the turbulent heat flux components (section 3.2), the estimation of wind stress (section 3.3), and the estimation of THFs (section 3.4) which vary in each parametrization due to the different computation of the bulk transfer coefficients. Then we discuss the role of the SST-Q_T negative feedback at play in the online prognostic SST approach comparing our results with Brodeau et al. (2017) (section 3.4). Except for sections 3.1 and 3.2, we consider only experiments which estimate the NSHFs using $T_s = SST$ in order to disentangle the THFs and wind stress differences contribution to the prognostic SST without the effect of the CSWL implementation.

3.1 Parametrization-related SST discrepancies

Figure 2 shows the differences in the TASFs, total turbulent heat fluxes Q_T and wind stress τ, from ECMWF_S and COARE_S with respect to NCAR. The TASFs drive substantial SST differences between experiments (Figure 3). While the SST in

https://doi.org/10.5194/gmd-2021-436
Preprint. Discussion started: 10 January 2022
© Author(s) 2022. CC BY 4.0 License.

COARE_S is warmer than in NCAR everywhere, the SST in ECMWF_S is overall warmer than in NCAR, but with a colder area (down to -0.6°C) over Eastern Boundary Upwelling Systems (EBUS) and over Pacific and Atlantic equatorial regions. In these experiments, which differ only in the bulk parametrization, the SST differences can arise from the differences in the wind stress and in the THFs as computed by the chosen bulk parametrization. In particular, the wind stress discrepancies, due to the computation of C_D and to the inclusion of the convective gustiness, may impact on the ocean dynamics by modifying the 3D ocean circulation and hence the pattern of the SST. The differences in THFs, due to the C_E and C_H computation and to the cool-skin/warm layer CSWL scheme, may affect the SST through modification of the heat loss to the atmosphere (dominated by evaporation in this region). Furthermore, differences in the wind stress and in THFs may also act together by amplifying or damping their single effect on the SST. Hereinafter, we focus on the differences between NCAR and ECMWF_S due to the substantial differences in SST between the two experiments (Figure 3).

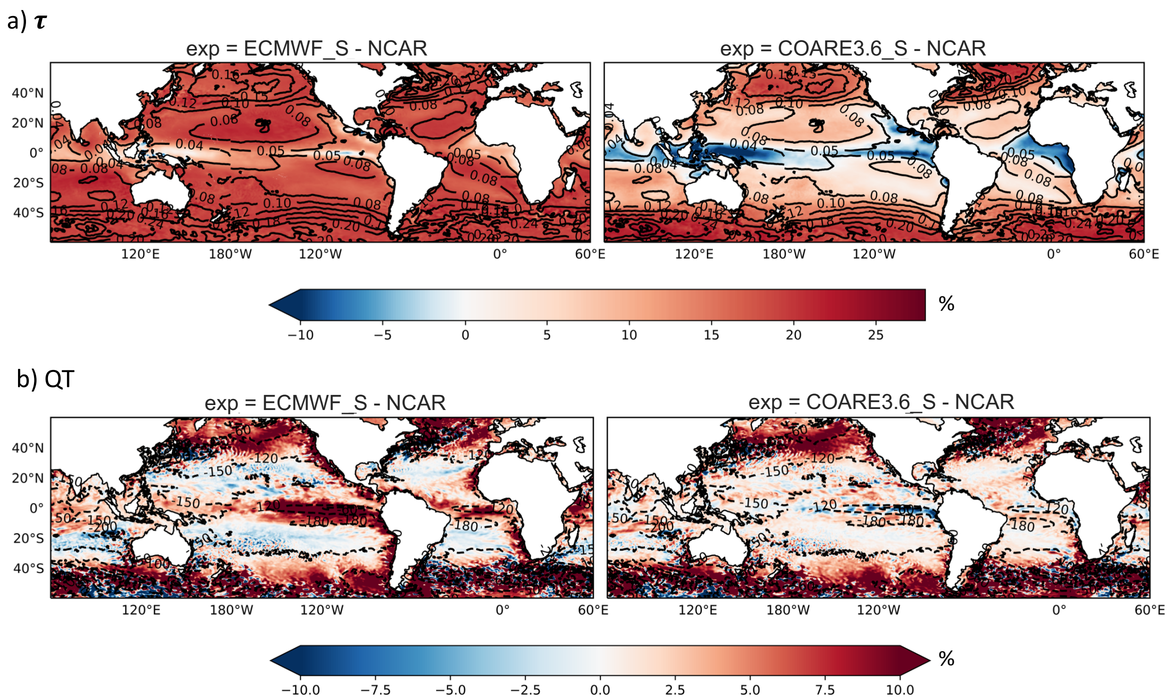

Figure 2. Annual mean differences between experiments of a) wind stress and b) total heat fluxes between ECMWF_S and NCAR experiments (left) and COARE_S and NCAR experiments (right). Contours are annual mean from NCAR experiment.

3.2 Skin temperature

The ECMWF and COARE parametrizations, in contrast to NCAR, expect SSTskin as the surface temperature input in order to estimate the near surface atmospheric stability and to compute the THFs. The SSTskin is also used to estimate the upward

https://doi.org/10.5194/gmd-2021-436
Preprint. Discussion started: 10 January 2022
© Author(s) 2022. CC BY 4.0 License.
Geoscientific Model Development
Open Access
Discussions

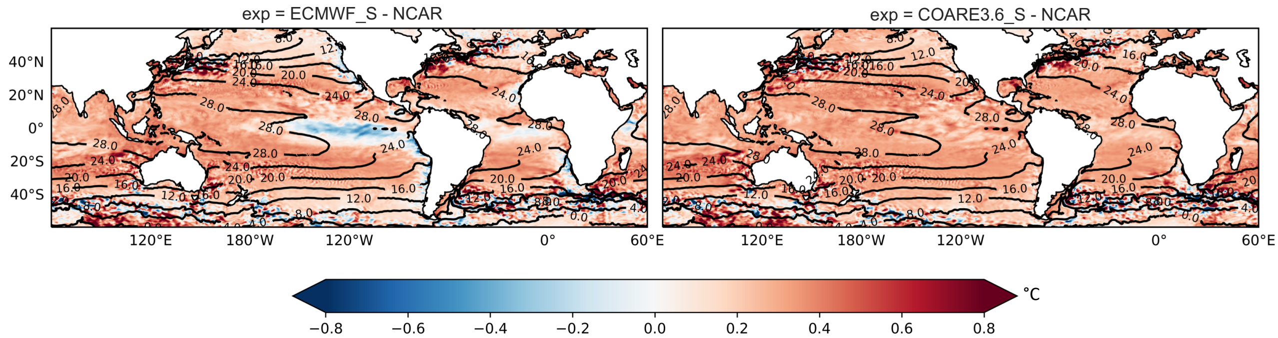

Figure 3. Annual mean SST differences between experiments (ECMWF_S-NCAR and COARE_S - NCAR, from left to right). Contours are annual mean SST from NCAR experiment.

long wave flux, needed by the CSWL scheme as components of the non solar heat flux. Here, we compare the results between ECMWF_S and ECMWF_NS to understand the impact of the CSWL implementation in driving the differences in the heat fluxes and by consequence in the SST shown in Figure 3 (see Table 1 for experiments details). We discuss the impact of the use of skin temperature for ECMWF parametrization, but similar results are found using COARE (not shown). The ECMWF_S experiment uses the CSWL scheme, so that $T_s \equiv SSTskin$ is used to compute THFs, as opposed to ECMWF_NS in which $T_s \equiv SST$. Consideration of the CSWL effect yields a SST global mean warming of 0.2°C (Figure 4c), with a maximum of 0.3°C over the western equatorial Pacific Ocean, in the Indo-Pacific Warm Pool. In the tropical eastern and Northern Pacific Ocean, and over Antarctic Circumpolar Current (hereinafter ACC), the differences are below 0.1°C. The global-mean SSTskin tends to be about 0.1°C colder than the SST (Figure 4a). On a global average basis, the cool skin process dominates over to the warm layer effect. Specifically, evaporation occurs almost everywhere and most of the time, while the warm layer builds up under sunny and low wind conditions.

The colder T_s in ECMWF_S with respect to ECMWF_NS yields a slightly weaker heat loss to the atmosphere due to the decreased NSHFs (mostly evaporation). In ECMWF_S the weaker heat loss to the atmosphere implies a gain of heat by the ocean (positive regions in Figure 4b) of approximately $1W/m^2$ on global average compared to ECMWF_NS. The negative SST discrepancies between parametrizations noted in Section 3.1 (Figure 3a) are not explained by the use of the CSWL scheme in the ECMWF parametrization. In particular, the SST differences between ECMWF_NS and NCAR (Figure 5a) with respect to the SST differences between ECMWF_S and NCAR (Figure 3) present a reduction of the overall warm temperature differences, but maintaining the cold temperature difference over the tropical Pacific and Atlantic and over the EBUS .

3.3 Turbulent Heat fluxes

In order to investigate the effect of the different computation of the THFs between ECMWF_S and NCAR in driving SST differences (Figure 5a), we compare the results between CdNCAR_CeEC and NCAR (see Table 1 for experiments details).

https://doi.org/10.5194/gmd-2021-436
Preprint. Discussion started: 10 January 2022
© Author(s) 2022. CC BY 4.0 License.

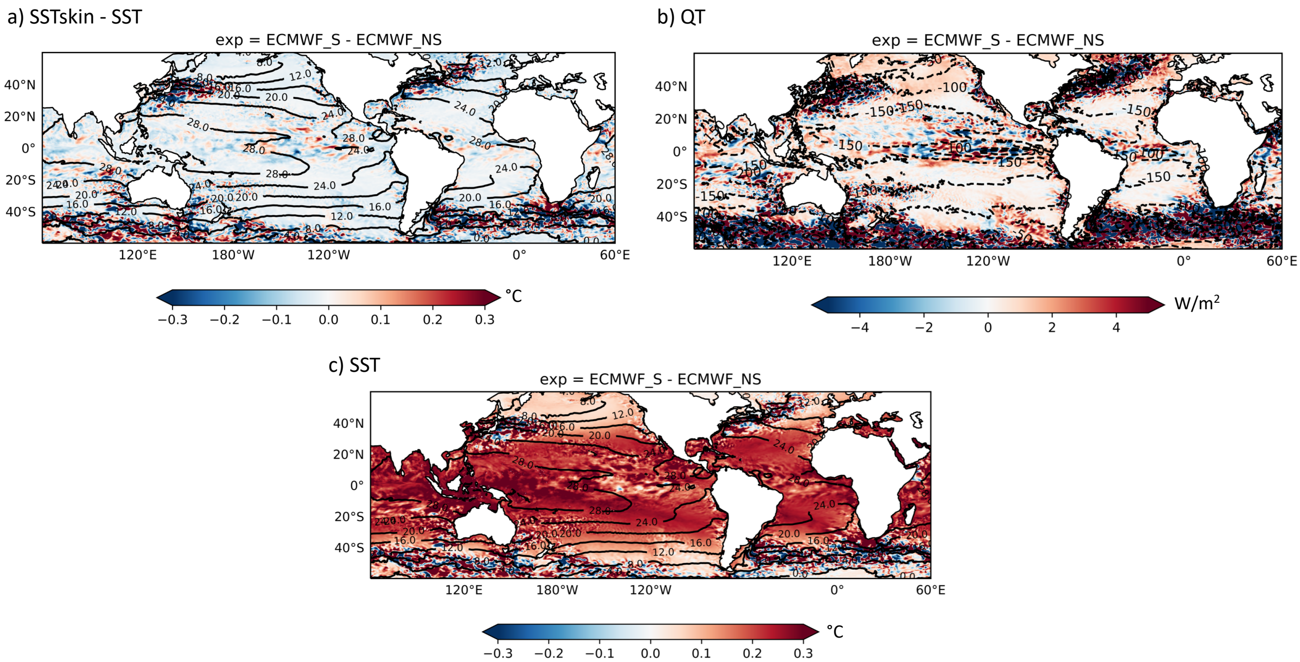

Figure 4. Annual mean differences of a) SSTskin-SST, b) total heat fluxes and c) SST between ECMWF_S- ECMWF_NS. Contours are annual mean from ECMWF_NS experiment

The SST differences between CdNCAR_CeEC and NCAR does not show SST differences pattern over EBUS and over equatorial Atlantic and Pacific ocean of the magnitude that we found between experiments ECMWF_S and NCAR (compare Figure 3a with Figure 5c). Over those areas, the SST in CdNCAR_CeEC is warmer than in NCAR of about 0.3°C on average. As shown in Figure 6a, CdNCAR_CeEC receives an excess of Q_T of about $10\,W/m^2$ on average with respect to NCAR. The main contributor to this difference is the latent heat (compare Figure 6a with Figure 7b), resulting from the difference in C_E in the two experiments. As previously discussed in section 2.2, the C_E of CdNCAR_CeEC, which is estimated by means of the ECMWF parametrization, underestimates the evaporation with respect to the C_E of NCAR (Figure 7a). This leads to an increased input of heat to the ocean in CdNCAR_CeEC. The differences in Q_T and SST have the same sign, which suggests that the Q_T drive the SST differences. As it is clearly shown by the annual zonal-mean differences time-series (Figure 6b): the higher the heat input in CdNCAR_CeEC along the latitude, the warmer the ocean modeled by CdNCAR_CeEC experiment with respect to NCAR.

In summary, weak evaporation, and by consequence, higher heat absorption in CdNCAR_CeEC generates an ocean surface that is warmer than NCAR. This result suggests that the wind stress differences between ECMWF_S and NCAR is the main driver of the cold SST pattern differences in Figure 3a.

https://doi.org/10.5194/gmd-2021-436
Preprint. Discussion started: 10 January 2022
© Author(s) 2022. CC BY 4.0 License.
Geoscientific Model Development Discussions
Open Access
EGU

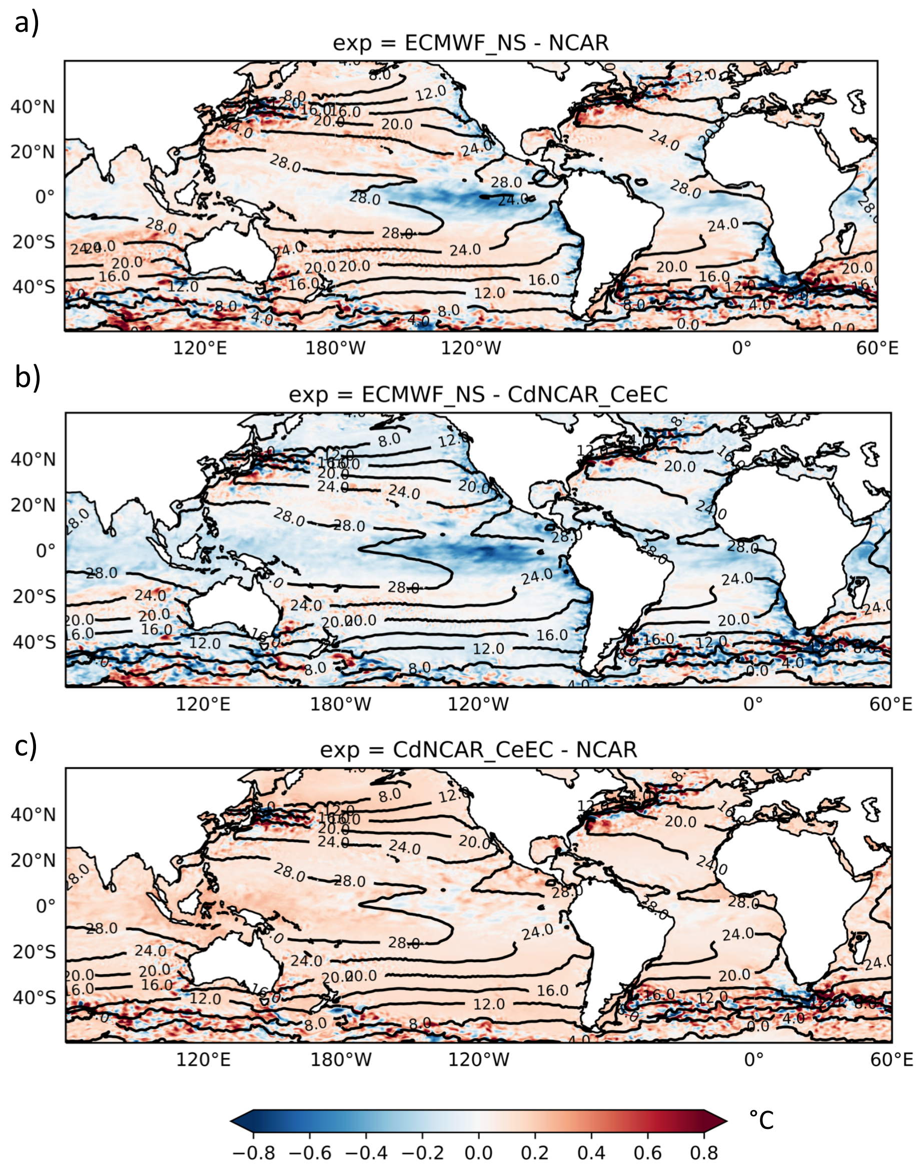

Figure 5. Annual mean SST differences between a) `ECMWF_NS - NCAR`, b) `ECMWF_NS - CdNCAR_CeEC`, c) `CdNCAR_CeEC - NCAR` . Contours are annual mean SST from `NCAR` experiment.

3.4 Drag coefficient and Wind stress

The impact of the wind stress computing by `ECMWF_S` and `NCAR` bulk parametrizations in driving the SST differences is here investigated by comparing results from `ECMWF_NS` and `CdNCAR_CeEC` simulations (see Table 1 for experiments details).

https://doi.org/10.5194/gmd-2021-436
Preprint. Discussion started: 10 January 2022
© Author(s) 2022. CC BY 4.0 License.

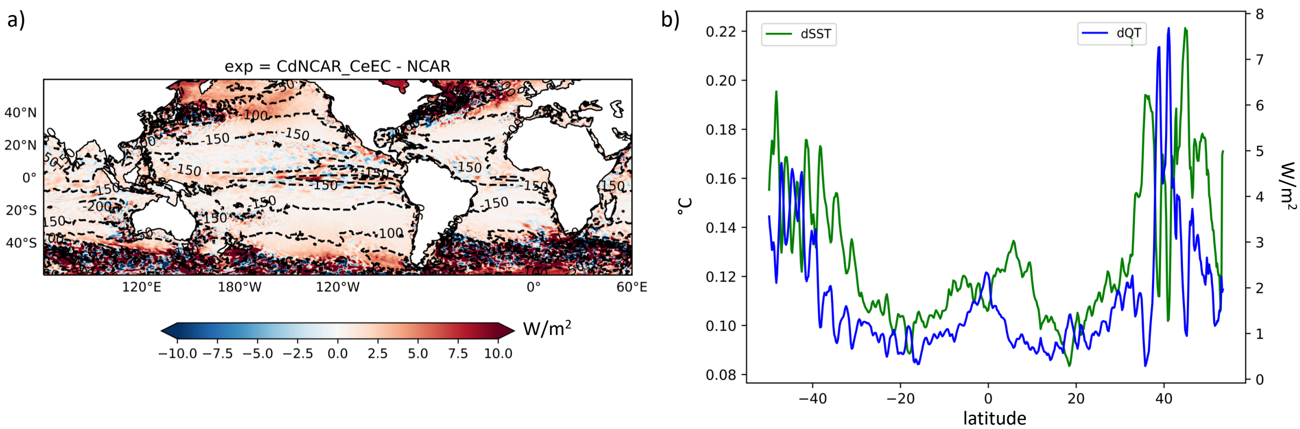

Figure 6. a) Annual mean differences of total heat fluxes QT between `CdNCAR_CeEC` and `NCAR` experiments. Contours are annual mean from `NCAR` experiment; b) time-series of differences in the annual zonal-mean of SST (green) and Q_T (blue) between `CdNCAR_CeEC` and `NCAR` experiments.

The SST simulated by `ECMWF_NS` is colder than `CdNCAR_CeEC` over EBUS and the tropical Pacific and Atlantic oceans (Figure 5a), regions characterized by wind driven upwelling. This suggests that wind stress is a major driver of the SST differences (Figure 3a). Referring to Equation 1a, the bulk formula estimates the wind stress as proportional to the wind speed vector at height z ($\mathbf{u_z}$), the bulk scalar wind speed $|\mathbf{u_z}|$ (with the potential inclusion of a gustiness contribution u), and the drag coefficient (C_D). Including gustiness in the ECMWF calculation produces the scalar wind differences in Figure 8a. As expected, the differences caused to gustiness emerge in regions with calm and unstable conditions. They are indeed located in the (5°N - 10°N) latitude band, in the eastern Pacific and Atlantic oceans, in the tropical western Pacific including the southern China Sea and the tropical Indian Ocean (compare contours and shaded areas in Figure 8a). These differences do not exceed $0.3m/s$.

Differences of C_D and C_D^{N10} fields between experiments show similar patterns (Figure 8b-c), suggesting that the differences in C_D between parametrizations are related to the neutral coefficient (C_D^{N10}) calculation rather than to its stability correction (term to add to C_D^{N10} to get C_D coefficients). Indeed, as discussed in section 2.2 for C_D^{N10}, the ECMWF C_D is larger than NCAR for wind speeds above 5 m/s, smaller than NCAR for calm up to light breeze conditions (U < 5 m/s). In the areas where U is approximately 4-5 m/s, such as in the north-west Pacific and Atlantic ocean (between 20°N and 30°N) and in the south-east Pacific and Atlantic ocean (between 20°S and 30°S), the ECMWF C_D is similar or slightly smaller than NCAR.

Since the wind stress is not affected by the type of first-order feedback at play for the NSHFs (SST-Q_T negative feedback driven, see section 2.2), differences of U and the C_D between experiments are reflected onto the resulting different fields after bulk calculation (i.e. τ and curl(τ), Figure 9). In particular, over the ACC, the northern and southern mid-latitudes (e.g. EBUS), and the Atlantic storm track (i.e regions characterized by wind speeds above $5m/s$ and `ECMWF_NS` C_D larger than

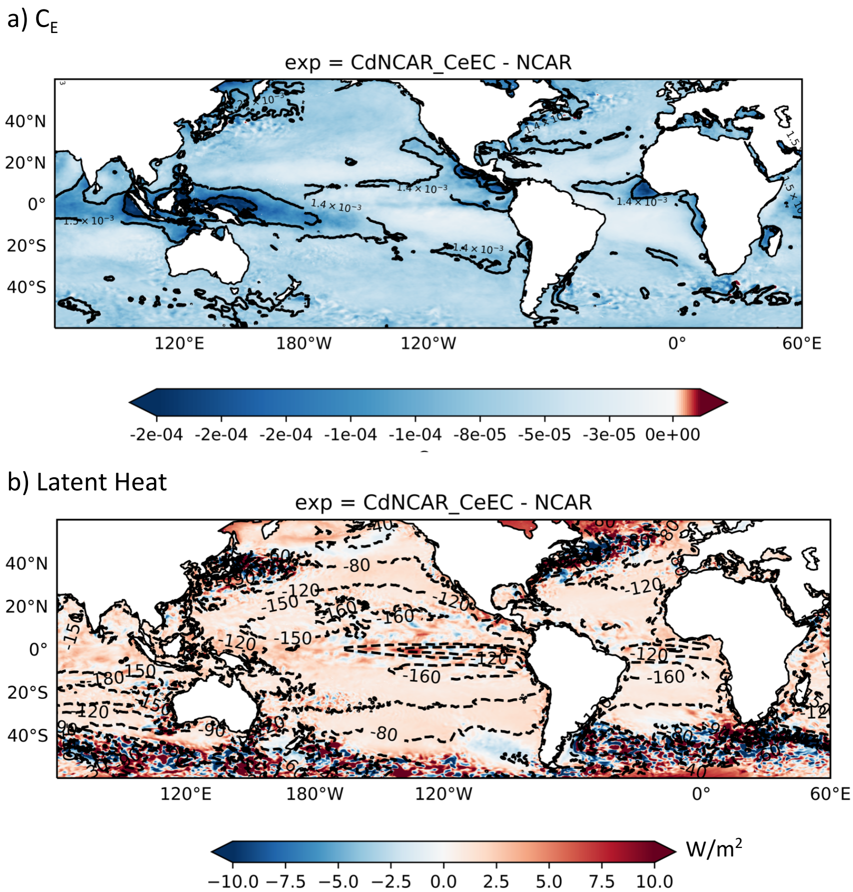

Figure 7. Annual mean differences of a) specific humidity transfer coefficient (C_E) and b) latent heat between CdNCAR_CeEC and NCAR experiments. Contours are annual mean from NCAR experiment.

CdNCAR_CeEC C_D, see Figure 8), the ECMWF_NS wind stress is stronger by about 20% with respect to NCAR. In the (5°N - 10°N region, latitudinal band characterized by mean winds below $5m/s$ and C_D larger in CdNCAR_CeEC than ECMWF_NS (Fig. 8), ECMWF_NS shows a wind stress reduction of about 3% with respect to NCAR. In regions where the differences in C_D are very small (i.e. the north-west and south-west Pacific and Atlantic ocean), the inclusion of convective gustiness in the U calculation generates the wind stress differences, leading an increase of the wind stress in ECMWF_NS. Therefore, the stronger wind stress along EBUS in ECMWF_NS compared to CdNCAR_CeEC, likely enhances coastal upwelling, explaining most of the SST differences over these regions. Part of the SST difference could be also related to Ekman suction, which is driven by the positive (negative) wind stress curl in the northern (southern) hemisphere. ECMWF_NS shows stronger positive (negative) wind stress curl in the northern (southern) hemisphere EBUS compared to CdNCAR_CeEC (Figure 9b). The SST differences between ECMWF_NS and CdNCAR_CeEC over the tropical Pacific and Atlantic Oceans (Figure 5) are instead related only to

https://doi.org/10.5194/gmd-2021-436
Preprint. Discussion started: 10 January 2022
© Author(s) 2022. CC BY 4.0 License.

Ekman suction. Substantial differences are found in ECMWF_NS compared to CdNCAR_CeEC, characterized by greater mean wind stress both north and south of the tropical band and weaker wind stress along the equator (Figure 9a). These latitudinal differences of the wind stress between experiments reflect in the differences in the wind stress curl patters (Figure 9b). Indeed, a stronger acceleration (deceleration) of southeast trades north (south) of the equator in ECMWF_NS may lead to a stronger positive (negative) curl north (south) of the Equator (Chelton et al., 2001).

Even though the two experiments use the same C_E and C_H, the dependence of Q_L and Q_H to the prognostic SST at each time-step generates differences in Q_T (Figure 10a). The ocean gains heat in ECMWF_NS compared to CdNCAR_CeEC (i.e. positive Q_T differences) over the EBUS and the Equatorial region. In contrast to the previous finding, the differences in Q_T and SST have opposite sign, indicating that SST differences drives the Q_T differences: the colder the temperature produced by ECMWF_NS wind stress with respect to CdNCAR_CeEC, the higher the heat gained by ECMWF_NS along the latitudes (Figure 10b).

In summary, ECMWF_NS reproduces stronger wind stress and wind stress curl along EBUS, and stronger cyclonic wind stress curl along the Equator, that generates colder SST with respect to CdNCAR_CeEC, through enhanced upwelling processes.

In light of the importance of the wind stress in driving the SST differences between ECMWF and NCAR parametrizations, we discuss why COARE_S does not display the cold SST differences in comparison to NCAR over EBUS and equatorial Pacific (Figure 3b). With wind speed ranging from 7 to 9 m/s (e.g. over EBUS) the C_D in COARE parametrization is smaller than that of ECMWF parametrization, but slightly higher or almost identical (around 7 m/s) to the C_D of NCAR (refer to Figure 1). Moreover, over the northern equatorial band the C_D of COARE is smaller than that of ECMWF and NCAR. As a consequence, the COARE_S differences in wind stress (Figure 2b) in comparison with NCAR are characterized by a strong decrease, roughly 10%, over the northern equatorial band and a slightly increase of the wind stress, roughly 2%, over EBUS. The increase of wind stress over EBUS in COARE_S (2% in comparison to 25% in ECMWF_S) is not enough to promote stronger coastal upwelling in the annual mean, and in turn colder SST with respect to NCAR. As regard the equatorial upwelling, the missed increasing of the wind stress north to the equator (e.g. northern equatorial cold front, Figure 2b) compared to NCAR wind stress, as we instead noticed for ECMWF_S (Figure 2a or Figure 9a), prevents the enhancement of the positive wind stress curl north to the equator. These considerations confirm that the wind stress differences, which derive from C_D differences, drive the SST differences across experiments, especially along wind driven areas.

3.5 Online prognostic SST approach vs offline prescribed SST approach

In order to discuss the role of the SST-Q_T negative feedback at play in the online prognostic SST approach, we compare our results with Brodeau et al. (2017), who compared the different bulk parametrizations using the offline prescribed SST approach (i.e. TASFs are computed by means of bulk formulas using prescribed surface atmospheric state variables and prescribed SST). They report a mean global increase of the wind stress of $20 mN/m^2$ using ECMWF parametrization instead of NCAR parametrization. The computation of the wind stress is not affected by the SST-Q_T negative feedback (see equation 1a), so that our results of $20 mN/m^2$ global mean increase of wind stress is completely in line with the prescribed SST comparison by Brodeau et al. (2017). Our findings do not follow Brodeau et al. (2017) in terms of the Q_T differences between ECMWF_S

https://doi.org/10.5194/gmd-2021-436
Preprint. Discussion started: 10 January 2022
© Author(s) 2022. CC BY 4.0 License.
Geoscientific Model Development
Discussions

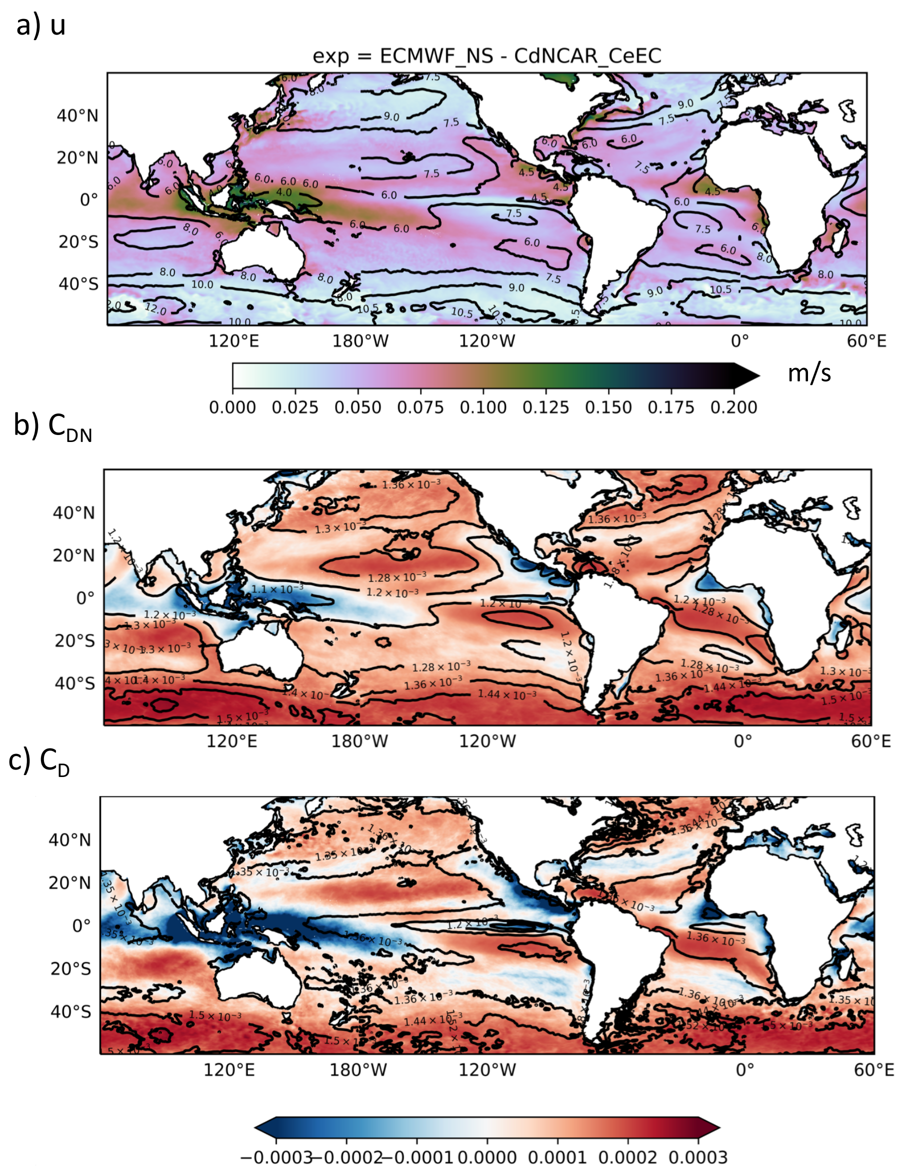

Figure 8. Annual mean differences of a) wind speed (U), b) neutral wind stress transfer coefficient (C_{DN}) and c) wind stress transfer coefficient (C_D) between `ECMWF_NS - CdNCAR_CeEC`. Contours are annual mean from `CdNCAR_CeEC` experiment.

and `NCAR` parametrizations. They find a global mean increase of Q_T of $13W/m^2$ for `ECMWF_S`, while in our experiments `ECMWF_S` displays a mean global increase of $5W/m^2$ with respect to `NCAR`. Moreover, they report an increase of $7W/m^2$ considering SSTskin rather than SST in COARE parametrization, while in our experiments `ECMWF_S` displays a mean global increase of $1W/m^2$ with respect to `ECMWF_NS`. The negative feedback between the SST and the Q_T which is active in

https://doi.org/10.5194/gmd-2021-436
Preprint. Discussion started: 10 January 2022
© Author(s) 2022. CC BY 4.0 License.

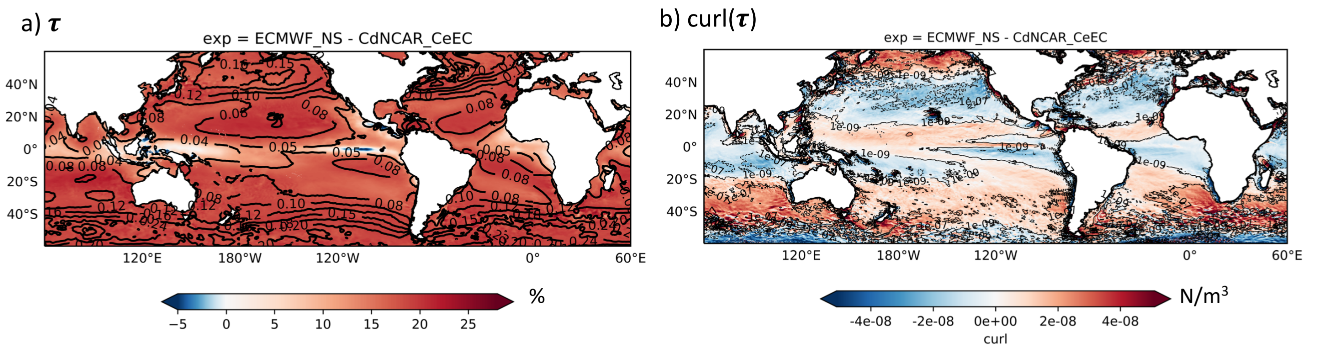

Figure 9. Annual mean differences of a) wind stress (τ) and b) curl of the wind stress ($curl(\tau)$) between `ECMWF_NS` - `CdNCAR_CeEC`. Contours are annual mean from `CdNCAR_CeEC` experiment.

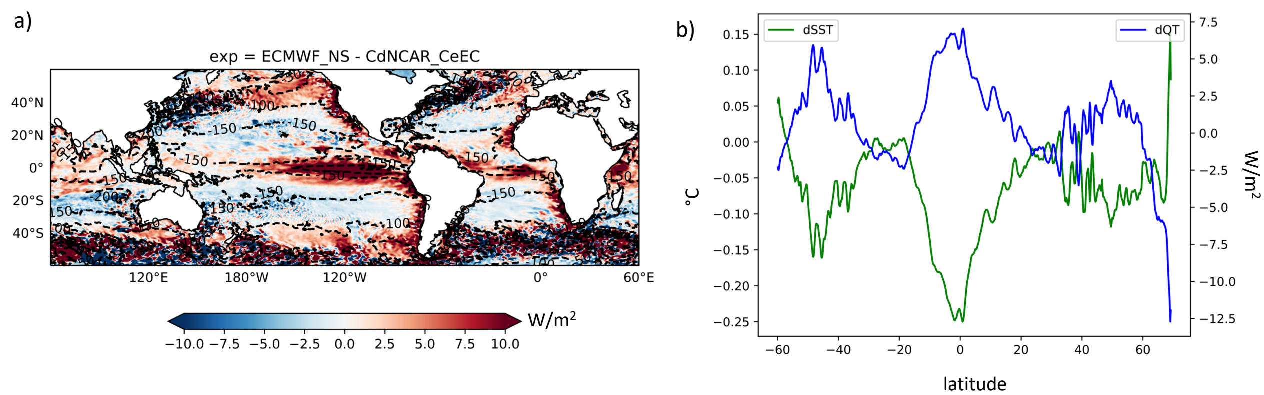

Figure 10. a) Annual mean differences of total heat fluxes (QT) between `ECMWF_NS` - `CdNCAR_CeEC`. Contours are annual mean from `CdNCAR_CeEC` experiment; b) Annual zonal-mean differences time-series of SST (green) and Q_T (blue) between `ECMWF_NS` - `CdNCAR_CeEC`.

our experiments reduces the differences in the total turbulent flux across parametrizations compared to the prescribed SST comparison.

4 Summary and conclusions

In this work we have investigated how the implementation of different bulk parametrizations in NEMO4 ocean general circulation model drives substantial differences in prognostic sea surface temperature. Specifically, we studied the contribution of distinct aspects and assumptions of the different bulk parametrizations in driving the SST differences across numerical ex-

https://doi.org/10.5194/gmd-2021-436
Preprint. Discussion started: 10 January 2022
© Author(s) 2022. CC BY 4.0 License.
Geoscientific Model Development
Discussions

periments performed using NEMO global model configuration with 1/4° of horizontal resolution. Namely, we analyzed and quantified the role of the inclusion of the skin temperature in the computation of the turbulent heat flux components, and we also studied the role of the turbulent heat flux components and of the wind stress in driving the SST differences between parametrizations. In order to do that, we analysed differences betweeen 'control experiments', short-term numerical experiments which used the different bulk parametrizations implemented in NEMO4, and 'mixed experiments', short-term sensitivity experiments where bulk assumptions are excluded (e.g skin temperature) or bulk transfer coefficients are computed mixing the different bulk parametrizations (e.g. C_D from NCAR parametrization and C_E and C_H from ECMWF parametrization). Moreover, the relevance of this work, other than highlighting the sensitivity of the sea surface temperature to the bulk parametrizations, is also to discuss the role of the SST-Q_T negative feedback at play in the simulations. As such, we compared the modeled turbulent air-sea fluxes with the estimations from Brodeau et al. (2017), who analyzed the same bulk parametrizations, but using offline prescribed SST approach. The findings can be summarized as follow:

1. The implementation of skin temperature in the bulk parametrizations reduces evaporation and decrease the turbulent heat flux to the atmosphere, promoting ocean warming (about 0.3°C on global average). The skin temperature is usually colder than the sea surface temperature. The skin temperature contribution in terms of turbulent heat flux is weaker with respect to the Brodeau et al. (2017) estimations. This is due to the SST feedback to the turbulent heat flux, in particular the negative feedback between the SST and the Q_T. In our experiments the SST is free to evolve and feeds back negatively with respect to Q_T.

2. The turbulent heat flux differences between experiments are dominated by the latent heat flux contribution, which derives from C_E differences between bulk parametrizations. Less evaporative ocean gains heat, which tends to promote ocean warming (about 0.1°C on global average). The turbulent heat flux differences are weaker with respect to the estimations of Brodeau et al. (2017) and they can be attributed to the SST-QT negative feedback.

3. The wind stress differences between bulk parametrizations are attributable to the C_D differences. The C_D differences result crucial especially along wind driven areas. In particular, strong wind stress or wind stress curl over EBUS and over Equatorial Pacific promote upwelling processes and consequent cooling of the sea surface temperature (about 0.4°C on global average). The wind stress differences across the bulk parametrizations implemented in NEMO4 result of the same magnitude of the wind stress differences calculated by Brodeau et al. (2017). This is due to the fact that, at the first order, the wind stress computation is not affected by the SST.

It is worth underlining that we are using forced ocean experiments in which the atmospheric fields (e.g. wind, air temperature, air humidity) given to the ocean model and seen in the online prognostic SST approach come from an atmospheric reanalysis, and do not respond back to the ocean variability. Introducing the air-sea feedback in the system might substantially impacts the turbulent fluxes and modify our finding in comparing the SST response among the bulk parametrizations. In the prospective of improving the representation of air-sea interaction in the NEMO framework, an atmospheric boundary layer (ABL) will be integrated in the NEMO release 4.2 (release scheduled for the end of 2021) and it will improve the representation of feedbacks

© Author(s) 2022. CC BY 4.0 License.

between the two components (Lemarié et al. (2020)). Currently, the ABL implementation is in a preliminary stage and the current online prognostic SST approach is still the favourit.

Appendix A: List of Acronyms

Acronym	Expansion
TASFs	Turbulent Air-Sea Flux components
THFs	Turbulent heat flux components
NSHFs	Non solar heat flux component
Q_T	Total turbulent heat flux
BTC	Bulk Transfer Coefficient
SSTSkin	Sea Surface Skin Temperature
CSWL	Cool Skin and (diurnal) Warm Layer
EBUS	Eastern Boundary Upwelling Systems

Code and data availability. The NEMO code used in this work is available at https://forge.ipsl.jussieu.fr/nemo/wiki/Users, version number: 12957. Model output is available upon request from Giulia Bonino (giulia.bonino@cmcc.it)

Author contributions. GB, DI and LB conceived the study. GB set up the experiment and improved the model. GB performed the analysis and wrote the manuscript. GB, DI and LB interpreted the results. All authors contributed to improving the manuscript.

Competing interests. The authors declare that they have no conflict of interest.

Acknowledgements. We acknowledge the CMCC Foundation for having provided computational resources.

https://doi.org/10.5194/gmd-2021-436
Preprint. Discussion started: 10 January 2022
© Author(s) 2022. CC BY 4.0 License.

References

Amante, C. and Eakins, B. W.: ETOPO1 arc-minute global relief model: procedures, data sources and analysis, 2009.

Barnier, B.: Forcing the ocean, in: Ocean modeling and parameterization, pp. 45–80, Springer, 1998.

Bernard, B., Madec, G., Penduff, T., Molines, J.-M., Treguier, A.-M., Le Sommer, J., Beckmann, A., Biastoch, A., Böning, C., Dengg, J., et al.: Impact of partial steps and momentum advection schemes in a global ocean circulation model at eddy-permitting resolution, Ocean dynamics, 56, 543–567, 2006.

Bonino, G., Iovino, D., and Masina, S.: Bulk Formulations in NEMOv.4:algorithms review and sea surface temperature response in ORCA025case study, Technical Notes No. 289, https://doi.org/10.25424/cmcc/bulk_formulas_nemo_report, 2020.

Bradley, E. and Fairall, C.: A guide to making climate quality meteorological and flux measurements at sea, 2007.

Brodeau, L., Barnier, B., Gulev, S. K., and Woods, C.: Climatologically significant effects of some approximations in the bulk parameterizations of turbulent air–sea fluxes, Journal of Physical Oceanography, 47, 5–28, 2017.

Chelton, D. B., Esbensen, S. K., Schlax, M. G., Thum, N., Freilich, M. H., Wentz, F. J., Gentemann, C. L., McPhaden, M. J., and Schopf, P. S.: Observations of coupling between surface wind stress and sea surface temperature in the eastern tropical Pacific, Journal of Climate, 14, 1479–1498, 2001.

Chen, D., Busalacchi, A. J., and Rothstein, L. M.: The roles of vertical mixing, solar radiation, and wind stress in a model simulation of the sea surface temperature seasonal cycle in the tropical Pacific Ocean, Journal of Geophysical Research: Oceans, 99, 20 345–20 359, 1994.

Dai, A. and Trenberth, K. E.: Estimates of freshwater discharge from continents: Latitudinal and seasonal variations, Journal of hydrometeorology, 3, 660–687, 2002.

Dai, A., Qian, T., Trenberth, K. E., and Milliman, J. D.: Changes in continental freshwater discharge from 1948 to 2004, Journal of climate, 22, 2773–2792, 2009.

ECMWF: Part IV: Physical Processes, no. 4 in IFS Documentation, ECMWF, https://www.ecmwf.int/node/9211, operational implementation 12 May 2015, 2015.

Edson, J. B., Jampana, V., Weller, R. A., Bigorre, S. P., Plueddemann, A. J., Fairall, C. W., Miller, S. D., Mahrt, L., Vickers, D., and Hersbach, H.: On the exchange of momentum over the open ocean, Journal of Physical Oceanography, 43, 1589–1610, 2013.

Fairall, C. W., Bradley, E. F., Rogers, D. P., Edson, J. B., and Young, G. S.: Bulk parameterization of air-sea fluxes for tropical ocean-global atmosphere coupled-ocean atmosphere response experiment, Journal of Geophysical Research: Oceans, 101, 3747–3764, 1996.

Fairall, C. W., Bradley, E. F., Hare, J., Grachev, A. A., and Edson, J. B.: Bulk parameterization of air–sea fluxes: Updates and verification for the COARE algorithm, Journal of climate, 16, 571–591, 2003.

Gill, A. E.: Atmosphere-ocean dynamics, Int. Geophys. Ser., 30, 662p, 1982.

Hersbach, H.: The ERA5 Atmospheric Reanalysis., AGUFM, 2016, NG33D–01, 2016.

IOC, I.: BODC. Centenary edition of the gebco digital atlas, Digital Media, 2003.

Jacobs, S. S., Hellmer, H. H., and Jenkins, A.: Antarctic ice sheet melting in the Southeast Pacific, Geophysical Research Letters, 23, 957–960, 1996.

Kara, A. B., Rochford, P. A., and Hurlburt, H. E.: Efficient and accurate bulk parameterizations of air–sea fluxes for use in general circulation models, Journal of Atmospheric and Oceanic Technology, 17, 1421–1438, 2000.

Large, W. and Pond, S.: Open ocean momentum flux measurements in moderate to strong winds, Journal of physical oceanography, 11, 324–336, 1981.

© Author(s) 2022. CC BY 4.0 License.

Large, W. and Pond, S.: Sensible and latent heat flux measurements over the ocean, Journal of physical Oceanography, 12, 464–482, 1982.

Large, W. and Yeager, S.: The global climatology of an interannually varying air–sea flux data set, Climate dynamics, 33, 341–364, 2009.

Lemarié, F., Samson, G., Redelsperger, J.-L., Giordani, H., Brivoal, T., and Madec, G.: A simplified atmospheric boundary layer model for an improved representation of air-sea interactions in eddying oceanic models: implementation and first evaluation in NEMO (4.0), Geoscientific Model Development Discussions, pp. 1–44, 2020.

Levitus, S., JI, A., OK, B., TP, B., CL, C., HE, G., AI, G., RA, L., AV, M., JR, R., et al.: The world ocean database, Data Science Journal, 12, WDS229–WDS234, 2013.

Madec, G. and Imbard, M.: A global ocean mesh to overcome the North Pole singularity, Climate Dynamics, 12, 381–388, 1996.

Madec G. and NEMO System Team: NEMO ocean engine, https://doi.org/10.5281/zenodo.1464816, 2019.

Marsaleix, P., Auclair, F., Floor, J. W., Herrmann, M. J., Estournel, C., Pairaud, I., and Ulses, C.: Energy conservation issues in sigma-coordinate free-surface ocean models, Ocean Modelling, 20, 61–89, 2008.

Monin, A. S. and Obukhov, A. M.: Basic laws of turbulent mixing in the surface layer of the atmosphere, Contrib. Geophys. Inst. Acad. Sci. USSR, 151, e187, 1954.

NEMO Sea Ice Working Group: Sea Ice modelling Integrated Initiative (SI^3) – The NEMO sea ice engine, https://doi.org/10.5281/zenodo.1471689, 2020.

Seager, R., Blumenthal, M. B., and Kushnir, Y.: An advective atmospheric mixed layer model for ocean modeling purposes: Global simulation of surface heat fluxes, Journal of climate, 8, 1951–1964, 1995.

Shriver, J. F. and Hurlburt, H. E.: The contribution of the global thermohaline circulation to the Pacific to Indian Ocean throughflow via Indonesia, Journal of Geophysical Research: Oceans, 102, 5491–5511, 1997.

Siedler, G., Griffies, S. M., Gould, J., and Church, J. A.: Ocean circulation and climate: a 21st century perspective, Academic Press, 2013.

Smith, S. D.: Coefficients for sea surface wind stress, heat flux, and wind profiles as a function of wind speed and temperature, Journal of Geophysical Research: Oceans, 93, 15 467–15 472, 1988.

Swenson, M. S. and Hansen, D. V.: Tropical Pacific Ocean mixed layer heat budget: The Pacific cold tongue, Journal of Physical Oceanography, 29, 69–81, 1999.

Torres, O., Braconnot, P., Marti, O., and Gential, L.: Impact of air-sea drag coefficient for latent heat flux on large scale climate in coupled and atmosphere stand-alone simulations, Climate Dynamics, 52, 2125–2144, 2019.

Yuen, C., Cherniawsky, J., Lin, C., and Mysak, L.: An upper ocean general circulation model for climate studies: Global simulation with seasonal cycle, Climate dynamics, 7, 1–18, 1992.

Zalesak, S. T.: Fully multidimensional flux-corrected transport algorithms for fluids, Journal of computational physics, 31, 335–362, 1979.